Finite element simulation of photoacoustic fiber optic sensors for surface rust detection on a steel rod

Qixiang Tang[a], Jones Owusu Twumasi[a], Jie Hu[a], Xingwei Wang[b] and Tzuyang Yu[a]
[a]Department of Civil and Enviromental Engineering
[b]Department of Electric and Computer Engineering
University of Massachusetts Lowell
One University Avenue, Lowell, MA 01854, U.S.A.

ABSTRACT

Structural steel members have become integral components in the construction of civil engineering infrastructures such as bridges, stadiums, and shopping centers due to versatility of steel. Owing to the uniqueness in the design and construction of steel structures, rigorous non-destructive evaluation techniques are needed during construction and operation processes to prevent the loss of human lives and properties. This research aims at investigating the application of photoacoustic fiber optic transducers (FOT) for detecting surface rust of a steel rod. Surface ultrasonic waves propagation in intact and corroded steel rods was simulated using finite element method (FEM). Radial displacements were collected and short-time Fourier transform (STFT) was applied to obtain the spectrogram. It was found that the presence of surface rust between the FOT and the receiver can be detected in both time and frequency domain. In addition, spectrogram can be used to locate and quantify surface rust. Furthermore, a surface rust detection algorithm utilizing the FOT has been proposed for detection, location and quantification of the surface rust.

Keywords: Finite element method (FEM), damage detection, surface rust, ultrasonic testing

1. INTRODUCTION

Non-destructive evaluation (NDE) is commonly used for monitoring and interrogating civil infrastructure systems. Ultrasonic testing (UT) is one of the most popular NDE techniques due to its reliability and accuracy.[1,2] However, successful ultrasonic wave generation and capturing require a good coupling between the transducers and the target. In cylindrical structures such as steel rods or pipes, the imperfect contact between a common transducer and the curve surface makes the application of UT challenging. Recently, a fiber optic transmitter (FOT) utilizing the photoacoustic effect has been proposed for generating ultrasonic waves as a point-source. Minimized FOT allows engineers to measure the conditions (e.g., temperature) of cylindrical structures without coupling issues.[3–6] To make this FOT applicable for detecting surface rust on a steel rod, a surface rust detection algorithm must be developed.

The purpose of this study is to investigate the point-source generated ultrasonic wave propagation in steel rods for detecting surface rust. In this work, ultrasonic wave propagation in steel rods was simulated using the finite element method (FEM). Ultrasonic wave propagation and effects of surface rust were analyzed by using time domain radial displacement ($u(t)$) and its spectrogram. A surface rust detection, localization and quantification algorithm was developed. The design of finite element models is first presented in the following section.

2. FINITE ELEMENT MODELS

Steel rod models were created with linear hexahedral elements (C3D8) using ABAQUS ®.[7] Corroded steel rod models were created by introducing an artificial surface rust anomaly to the intact steel rod model. Time domain radial displacement ($u(t)$) at the receiver of each model was collected and analyzed. Details of the models are described in the following.

Further author information: (Send correspondence to T. Yu)
E-mail: tzuyang_yu@UML.EDU, Telephone: 1 978 934 2288

Table 1. Material's properties

	Steel	Rust
Density (kg/m^3)	7850	2610
Youngs Modulus (MPa)	210,000	500
Poissons Ratio	0.3	0.3

2.1 Intact steel rod model

An intact steel rod model was created by generating a 50-mm long cylinder with a diameter (D) of 12.7 mm, as shown in Fig. 1. The intact steel rod model was made of steel with materials properties provided in Table 1. A transmitter was located at mid-span and denoted by T. A receiver (R) was located on the longitudinal axis (z-axis) of the steel rod. The distance from the transmitter to the receiver (s_1) was 10 mm. The two ends of rod were fixed. On each end of the rod, ten absorbing layers were applied to suppress unnecessary reflections.[8] When elastic waves propagated into the absorbing layers, they were damped out. The material property of absorbing layers was steel with additional damping. The damping coefficient of absorbing layers increases linearly from center region to the fixed end. A sinusoidal pulse (as shown in Fig.2) was applied at T as input loading. Time domain radial displacement ($u(t)$) was collected at R.

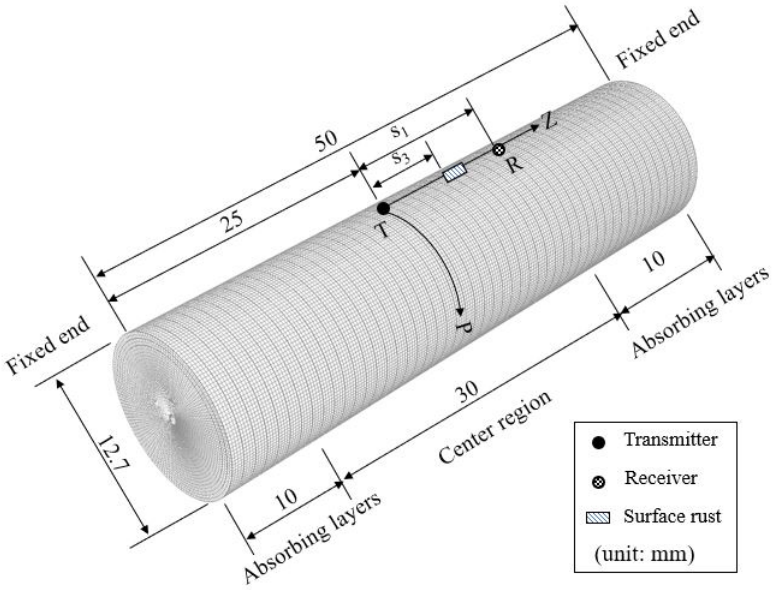

Figure 1. Intact steel rod model

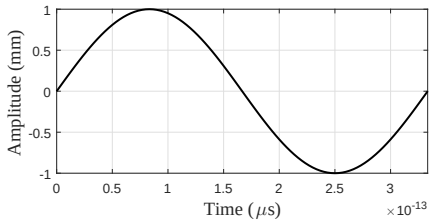

Figure 2. Loading function

Table 2. Considered corroded steel rod models

Model	Surface rust location s_3 (mm)	Surface rust length d (mm)	Surface rust width w (mm)	Surface rust thickness h (mm)
CM1	4	2	2	2
CM2	4	4	2	2
CM3	6	2	2	2

2.2 Corroded steel rod models

Corroded steel rod models were created by introducing surface rust to the intact steel rod model. Material properties were updated from steel to rust in the corroded region. To characterize surface rust, four attributes were defined: location s_3, length d, width w and thickness h. In this study, two different surface rust locations ($s_3 = 4$ mm and 6 mm, s_3 was measured from the center of surface rust) and two different surface rust lengths ($d = 2$ mm and 4 mm) were considered. Three corroded steel rod models were created: corroded steel rod model 1 (CM1), corroded steel rod model 2 (CM2) and corroded steel rod model 3 (CM3). Characteristics of surface rust in each corroded steel rod model are listed in Table 2.

2.3 Hypotheses of ultrasonic waves propagation in intact and corroded rod models

Based on the geometry of the intact and corroded rod models, hypotheses were made to predict ultrasonic waves propagation in intact and corroded rod models. Fig. 3 shows a Mercator projection of the rod surface. The hypotheses were:

- In the intact steel rod model, ultrasonic waves are generated at T. The first ultrasonic waves being collected by R is the one propagating along the $\vec{s}_1$ path. Its propagation velocity is c_1. The second ultrasonic waves being collected is the wave propagating along the $\vec{s}_2$ path and arrived R at t_2. Its propagation velocity is c_2.
- In the corroded steel rod model, the ultrasonic waves propagating along the $\vec{s}_1$ path encounter surface rust. Part of the ultrasonic waves propagates through the surface rust and gets delayed. It arrived R at t_1'. Higher frequency components of this part of the ultrasonic waves reduce. This is because surface waves such as Rayleigh waves interact with surface rust based on its effective depth, which is approximate to its relative wavelength.[9] Higher frequency components (smaller wavelength) have small effective depth and are affected more than lower frequency components do. Another part of the ultrasonic waves is scattered by surface rust and propagated along the $\vec{s}_4$ path. The time of flight (TOF) of scattered ultrasonic waves propagating along $\vec{s}_3$ and $\vec{s}_4$ is t_2' ($t_2' = t_3 + t_4$). c_1' and c_2' were defined as the average velocity of ultrasonic waves propagate on $\vec{s}_1$ and $\vec{s}_3$+$\vec{s}_4$.

Furthermore, based on the hypotheses, surface rust detection, localization and quantification can be achieved. The presence of surface rust leads to reduction of higher frequency components. Therefore, the detection of surface rust can be accomplished by comparing the greatest frequency component (f_h) at half-power level of spectrograms. The procedure of obtaining f_h from redial displacement $u(t)$ is reported in the following steps. (1) Collect the radial displacement $u(t)$; (2) Convert $u(t)$ to spectrogram using short-time Fourier transform (STFT); (3) Find the half-power level by subtracting 3 dB from the maximum amplitude of the first wave packet; and (4) Find the highest frequency component (f_h) of first wave packet in the contour at half-power level. As an example, Fig. 4 shows the procedure of obtaining f_h value from CM1. Once the f_h is found, Eq. (1) can be used for detecting the presence of surface rust.

$$\Delta f_h = f_{h,i} - f_{h,c} \begin{cases} = 0 & \text{intact} \\ \neq 0 & \text{corroded} \end{cases} \tag{1}$$

where Δf_h = the difference in the greast frequency component at half-power level between intact and corroded steel rod models (MHz), $f_{h,i}$= the greatest frequency component at half-power level in the intact steel rod model

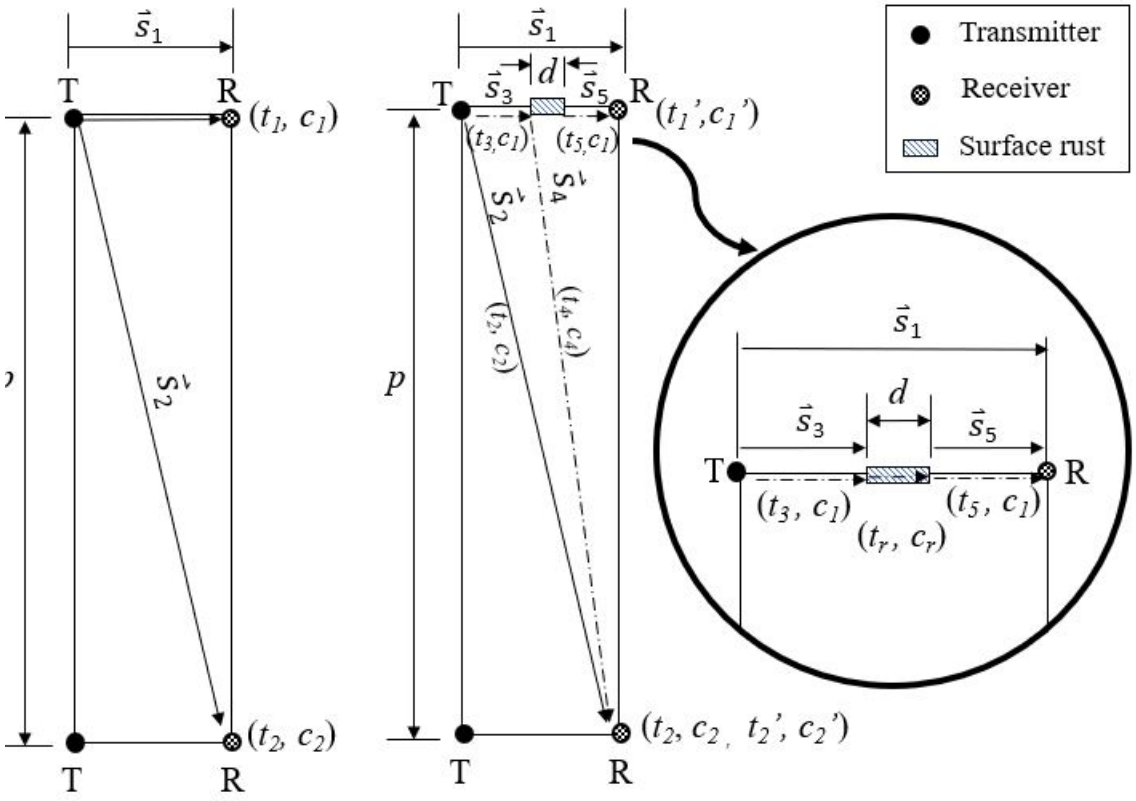

Figure 3. Ultrasonic wave propagating paths on Mercator projection of intact rod surface (left) and corroded rod surface (right)

(MHz), $f_{h,c}$ = the greatest frequency component at half-power level in the corroded steel rod model (MHz). Eq. (1) represents a model for detecting the presence of surface rust in the algorithm.

TOF of the scattered waves was the total propagation time of ultrasonic waves travel on $\vec{s}_3$ and $\vec{s}_4$. This relationship can be described by Eq. (2).

$$t_2'(s_3, s_4) = t_3 + t_4 = \frac{s_3}{c_1} + \frac{s_4}{c_4} \tag{2}$$

where t_4 = TOF of the ultrasonic waves propagate alone $\vec{s}_4$ (μs), c_4 = the surface wave velocity on the $\vec{s}_4$ path (mm/μs), $s_4(s_3)$ = the length of the $\vec{s}_4$ path (mm) = $\sqrt{(s_1 - s_3)^2 + p^2}$ and p = perimeter of the rod (mm).

TOF of the delayed waves in the intact steel rod model was a summation of TOF of ultrasonic waves travel on steel surface and in the surface rust. Eq. (3) described this relationship.

$$t_1'(d) = t_3 + t_r + t_5 = \frac{s_3 + s_5}{c_1} + \frac{d}{c_r} = \frac{s_1 - d}{c_1} + \frac{d}{c_r} \tag{3}$$

where t_1' = TOF of the ultrasonic waves propagate alone $\vec{s}_1$ in the corroded steel rod model (μs), t_3 = TOF of the ultrasonic waves propagate alone $\vec{s}_3$ (μs), t_r = TOF of the ultrasonic waves propagate in the surface rust (μs), t_5 = TOF of the ultrasonic waves propagate alone $\vec{s}_5$ (μs), s_1 = the distance between the FOT and the receiver (mm), c_1 = surface wave velocity on z-axis along $\vec{s}_1$ (mm/μs), c_r = the surface wave velocity on z-axis in rust = $0.08454{c_1}^9$(mm/μs) and d = length of surface rust (mm). After re-arranging Eq. (3), the surface rust length d can be calculated by Eq. (4).

$$d(t_1') = \frac{c_r s_1 - c_r c_1 t_1'}{c_r - c_1} \tag{4}$$

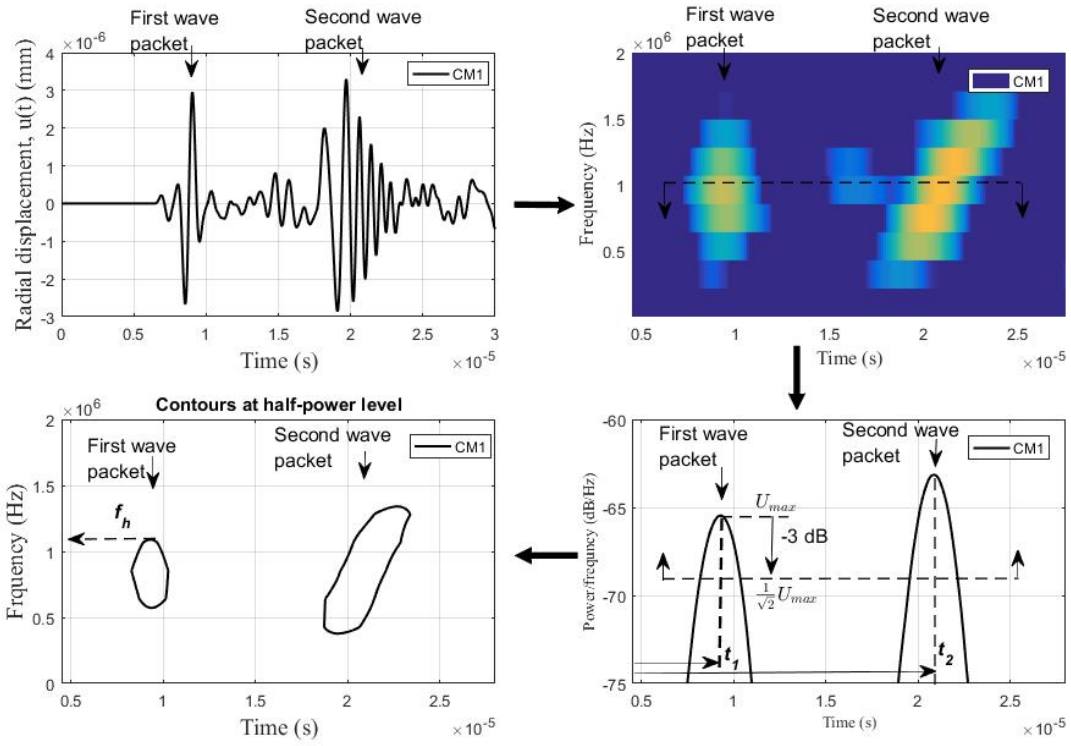

Figure 4. Procedure of obtaining f_h value

Eq. (4) represents a model for quantify the length of surface rust in the algorithm.

These hypotheses were used for developing a surface rust detection algorithm with the simulation results reported in the following section.

3. RESULTS

Radial displacement ($u(t)$) in the time domain of each model was collected, and STFT was applied to obtain the spectrogram of $u(t)$. Comparison (of $u(t)$ and spectrogram) between intact and corroded steel rod models was made. A surface rust detection algorithm was developed based on the findings of comparative study.

3.1 Time domain response

In the time domain, radial displacement ($u(t)$) of rod models was collected and shown in the Fig. 5. Two wave packets were observed. As stated in the hypotheses, the first wave packet was the waves propagating from the transmitter (T) to the receiver (R) along the longitudinal axis (z-axis). The second wave packet was the waves propagating along a helical path ($\vec{s_2}$ in Fig. 3). The second wave packet arrived later than the first one due to its longer path. In addition, the waveform of the second wave packet changed because of the dispersion effect caused by the rod geometry.

In the corroded rod models, the first peak amplitude (u_1) was found to be reduced comparing with the intact steel rod model. This was because part of the first wave packet was delayed by the surface rust. In addition, surface rust location leaded to more reduction of first peak amplitude than surface length does. For example, by shifting the rust location from s_3 = 5 mm to s_3 =7 mm, 20.2% of reduction was found in the first peak amplitude. With surface rust length increased from 2 mm to 4 mm, first peak amplitude reduction decreased for 8.08%. The reduction of first peak amplitude (Δu_1) was reported in Table 3.

The presence of surface rust was observed with first peak amplitude reduction. However, these observations were effected by the dispersion of ultrasonic waves. In addition, time domain signals were usually contaminated

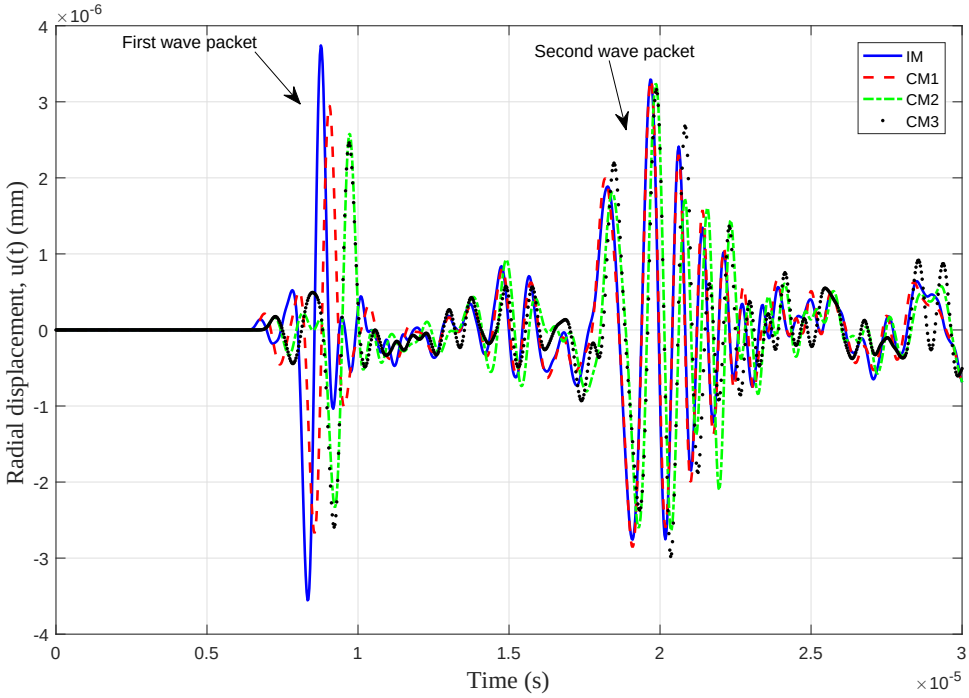

Figure 5. Time domain redial displacement in intact and corroded steel rod models

Table 3. First peak amplitude reduction of each corroded steel rod models

	First peak amplitude (u_1) ($\times 10^{-6}$ mm)	First peak amplitude reduction (Δu_1) ($\times 10^{-6}$ mm)	Difference from CM1
intact steel rod model (IM)	3.37	-	-
corroded steel rod model 1 (CM1)	2.38	0.99	-
corroded steel rod model 2 (CM2)	2.46	0.91	-8.08%
corroded steel rod model 3 (CM3)	2.58	0.79	-20.2%

by noises in practice. Analysis in the frequency domain was often utilized to deal with noises. Therefore, to develop a practical surface rust detect algorithm, STFT was applied to obtain both the time domain and the frequency domain information.

3.2 Spectrogram of intact and corroded steel rod models

By performing STFT to collected $u(t)$, change of frequency components over time was observed on spectrograms. During the application of the proposed FOT,[5] noises were found to be around 0.01 MHz and 8.5 MHz. Therefore, spectrograms of $u(t)$ in this study were limited between 0.1 MHz and 2 MHz. In the truncated spectrogram of responses at T in the intact steel rod model (Fig. 6), two wave packets was observed. The first wave packet was the input loading. When the ultrasonic waves were generated, all frequency components were generated simultaneously. Therefore, a vertical strip shape of this wave packet was shown in the spectrogram. The second wave packet, appeared around 20 μs, represented the ultrasonic waves after propagating along azimuth axis for one cycle and back to T. When ultrasonic waves propagating on a curved surface, ultrasonic waves become dispersive. Low-frequency component (i.e., frequency components lower than 1 MHz, $f < 1$ MHz) travels faster than high-frequency component ($f > 1$ MHz) and arrives at T earlier than high-frequency component. As a result, the shape of a second wave packet in the spectrogram plot was tilted.

In spectrogram of all models at R (Fig. 7), two wave packets were observed. The first wave packet, appearing around 8 μs, represented the ultrasonic waves propagates from T to R along the longitudinal axis (z-axis). The

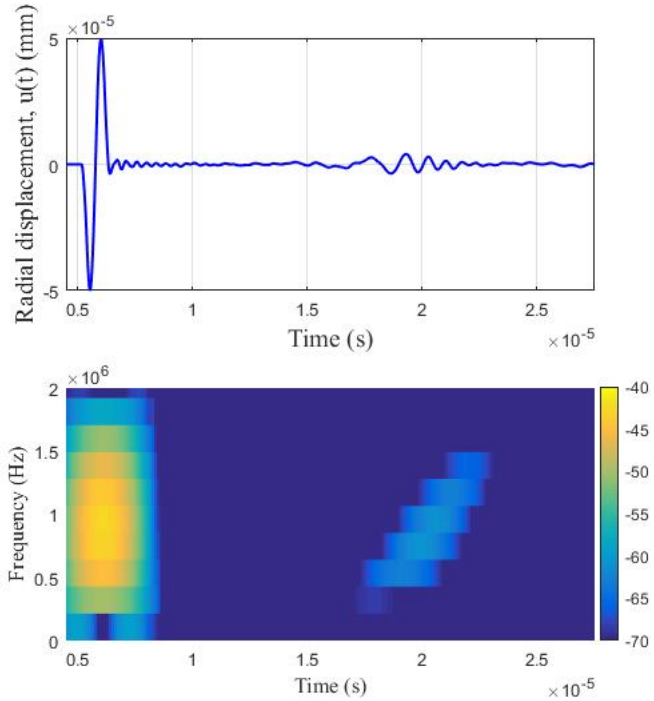

Figure 6. Radial displacement and spectrogram of the intact steel rod model at the transmitter

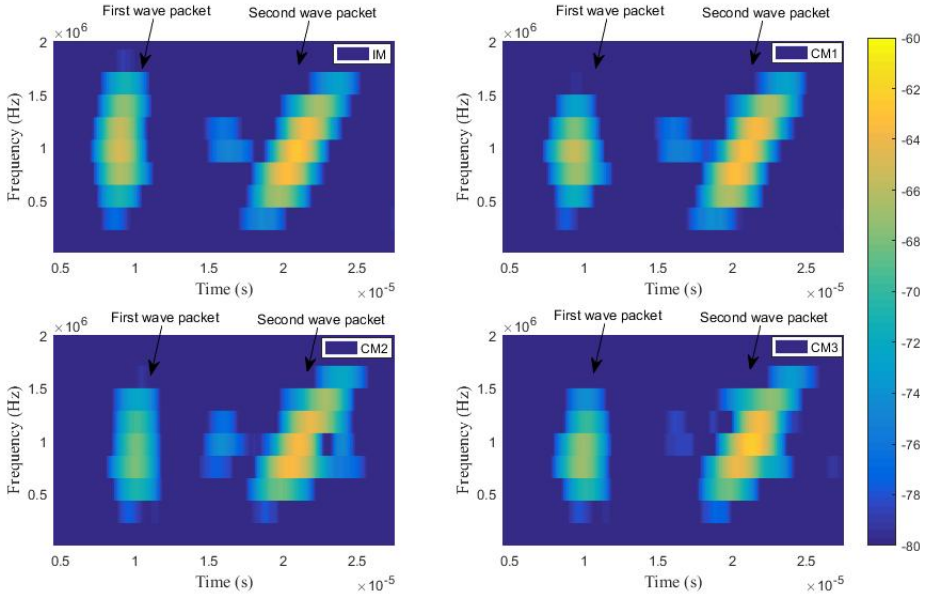

Figure 7. Spectrogram of intact and corroded steel rod models

second wave packet, appearing around 20 μs, represented the ultrasonic waves propagated for one cycle and arrives at R. In corroded steel rod models, high-frequency components in the first wave were reduced because effective depth of high-frequency components were short.

Fig.8 shows the contours of each spectrogram at three different levels (i.e., -67 dB, -70 dB and -73 dB) for between intact and corroded steel rod models. At -70 dB contour of CM1, the top part of the first wave packet

Table 4. Highest frequency component (f_h) in the contour at half-power level

	f_h (MHz)	Δf_h (MHz)
intact steel rod model (IM)	1.31	0
corroded steel rod model 1 (CM1)	1.09	0.22
corroded steel rod model 2 (CM2)	1.18	0.13
corroded steel rod model 3 (CM3)	1.08	0.23

was disappeared. This indicated the loss of high frequency components. In addition, extra waves were found at the end of the second wave packet. In CM2, the surface rust location shifted from $s_3 = 5$ mm to $s_3 = 7$ mm, the first wave packet had greater reduction in high-frequency components than in CM1, extra waves were also found after second wave packet.

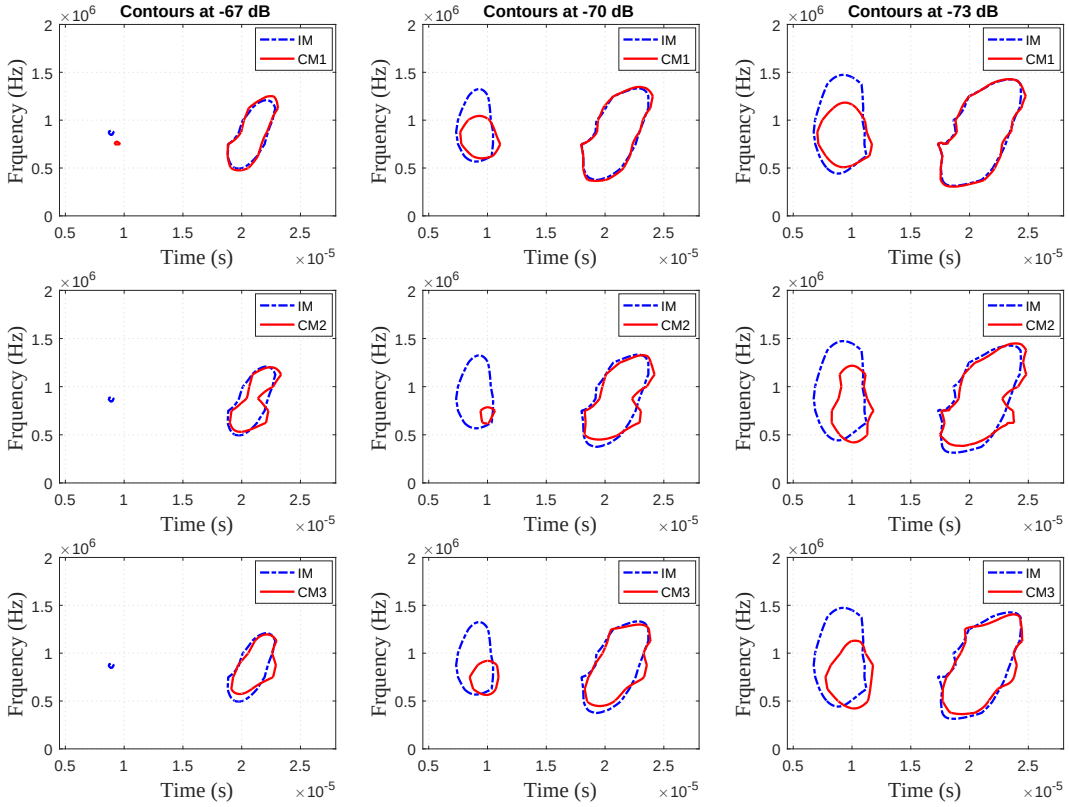

Figure 8. Contour of each spectrogram at -67 dB,-70 dB and -73 dB

3.3 Surface rust detection, localization and quantification

The detection of surface rust in a corroded steel rod model was accomplished by the comparing the highest frequency component (f_h) in the contour at half-power level, as shown in Fig. 9. Values of f_h and Δf_h of intact and corroded steel rod models were reported in Table 4. Δf_h of all corroded steel rod models were found to be non-zero. Based on Eq. (1), the presence of surface rust in these models were indicated.

Surface rust in a corroded steel rod model was localized using the relationship described by Eq. (2). However, due to the dispersion of ultrasonic waves, measuring TOF became difficult. To overcome the dispersion effect, only a particular frequency component (i.e., central frequency of the input loading, which was 1 MHz) was used. As an example, Fig. 10 presented the spectrogram at 1 MHz of the intact steel rod model and CM1. In the

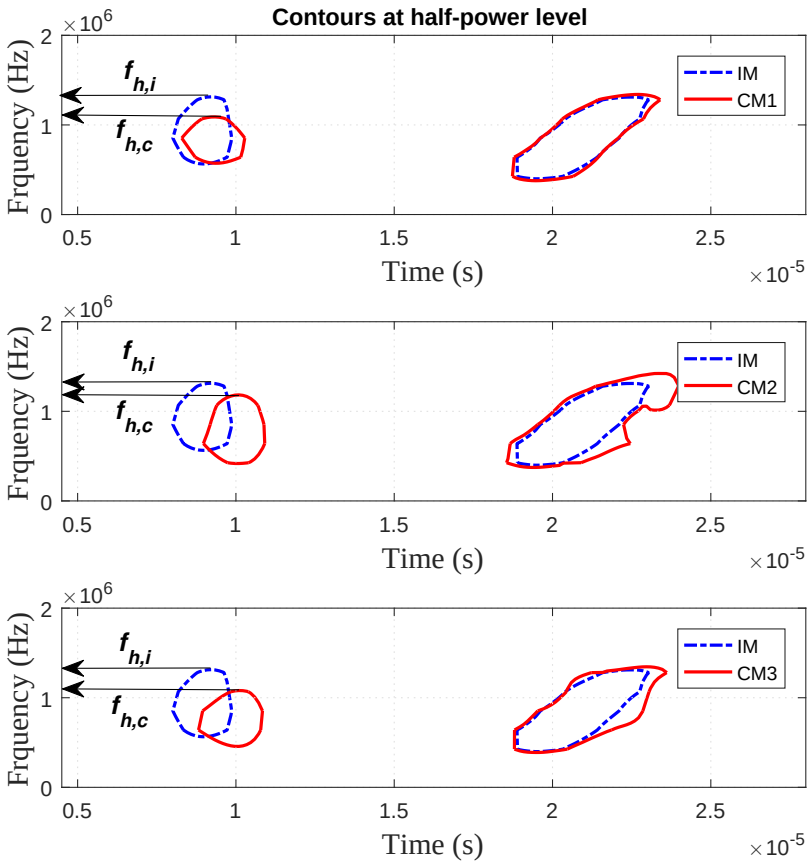

Figure 9. Contour of each spectrogram at -67 dB,-70 dB and -73 dB

intact steel rod model, t_1 and t_2 were estimated by computing the TOF of the peaks. t_1' and t_2' were difficult to be identified since they were overlapped with the other waves. By subtracting the spectrogram at 1 MHz of the intact steel rod model from the corroded steel rod models, t_1' and t_2' were found. In order to utilize Eq. (2), velocity of scattered ultrasonic waves (c_4) was required. Following steps were proposed to calculate c_4.

1. Compute ultrasonic waves c_0, c_1 and c_2 with information obtained in the intact steel rod model (i.e., t_0, p, t_1, s_1, t_2 and s_2), as shown in Fig. 11 (left).

2. Develop an equation (Eq. (5)) to descried the relationship between ultrasonic waves velocity (e.g., c_0, c_1 and c_2) and the angle of propagation path (θ), as shown in Fig. 11 (middle).

$$c(\theta) = 3.47 - 0.8348\sin(\theta) \tag{5}$$

3. Re-write Eq. (5) for corroded steel rod models. In corroded steel rod models, $\theta = \sin^{-1}\left(\frac{p}{s_4}\right)$, as shown in Fig. 11 (right). Substitute $\theta = \sin^{-1}\left(\frac{p}{s_4}\right)$, Eq. (5) was re-written in the following form.

$$c_4(s_4) = 3.47 - 0.8348\left(\frac{p}{s_4}\right) \tag{6}$$

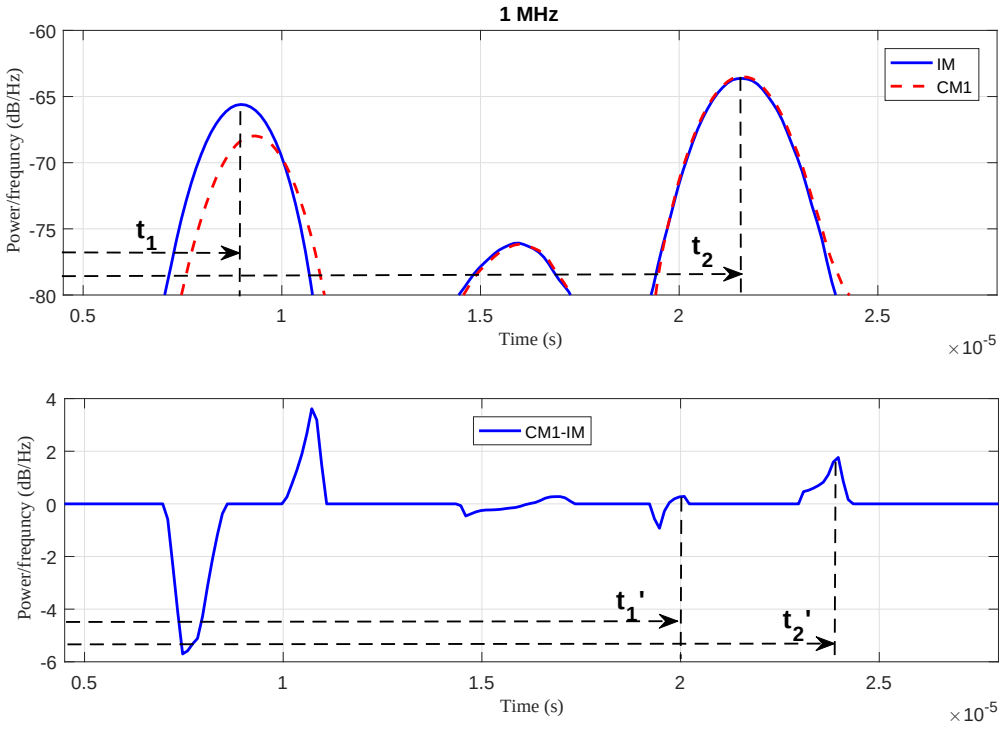

Figure 10. Spectrograms of the intact steel rod model and CM1 at 1 MHz

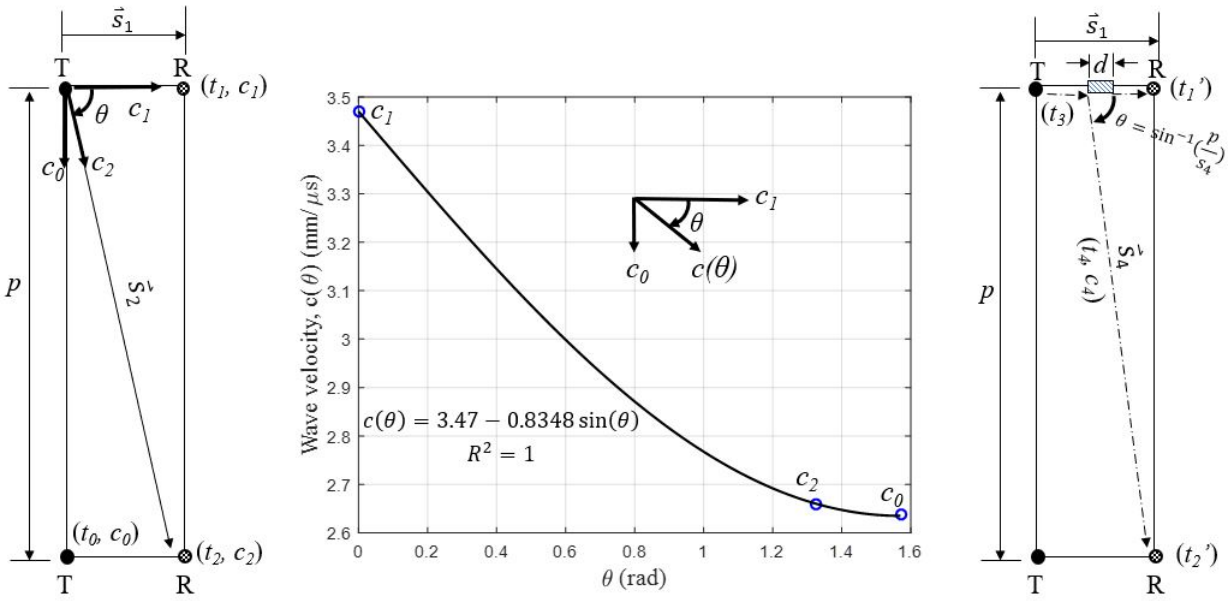

Figure 11. Wave velocity estimation for $c(\theta)$

Substituting Eq. (6) into Eq. (2), the relationship between t_2' and s_3 was expressed as Eq. (7). Eq. (7) represents

a model for locating the surface rust in the algorithm.

$$t_2'(s_3) = t_3 + t_4 = \frac{s_3}{c_1} + \frac{\sqrt{(s_1 - s_3)^2 + p^2}}{3.47 - 0.8348\left(\frac{p}{\sqrt{(s_1 - s_3)^2 + p^2}}\right)} \tag{7}$$

Fig. 12 showed the relationship s_3 and t_2'. It was directly used for localizing the surface rust once t_2' was measured from a corroded steel rod model. The estimated surface rust location s_3 of corroded steel rod models was also marked in Fig. 12. For CM1, estimated surface rust location s_3 was 3.86 mm, which was 3.5% error from the actual value in CM1. For CM2, estimated surface rust location s_3 was 2.92 mm, which was 2.6% error from the actual value in CM2. For CM3, estimated surface rust location s_3 was 5.91 mm, which was 3% error from the actual value in CM3.

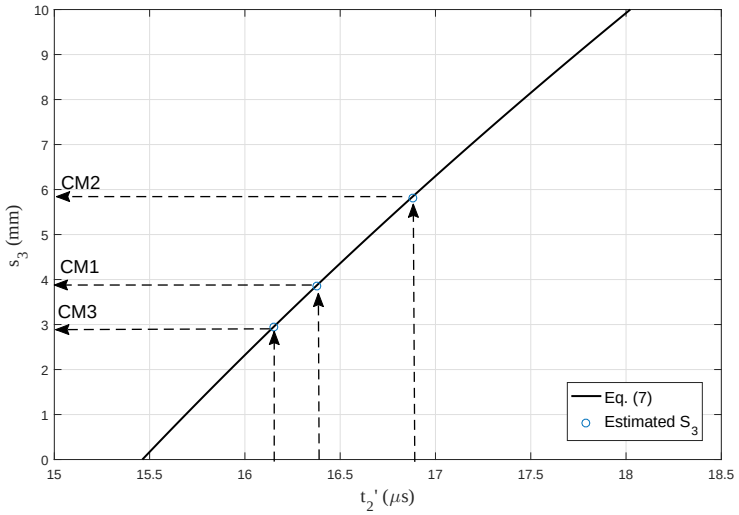

Figure 12. Relationship between s_3 and t_2'

Eq. (4) was applied to quantify the surface rust length. For CM1, estimated surface rust length d was 1.97 mm, which was only 1.5% error from the model. For CM2, estimated surface rust length d was 3.69 mm (7.75% error). For CM3, estimated surface rust length d was 2.1 mm (5% error).

By conducting the finite element analysis of ultrasonic waves propagation in intact and corroded steel rod models, following research findings were obtained: (1) In the time domain, the first peak amplitude (u_1) was reduced due to the presence of a surface rust; (2) In the spectrogram, because ultrasonic waves propagating dispersively (low-frequency component travels faster than high-frequency component), the shape of a second wave packet in the spectrogram plot was tilted; (3) The first wave packet in corroded steel rod models suffered from high frequency components loss. This was because high-frequency components (small wavelength) had small effective depth and were affected by surface rust more than low-frequency components; (4) In the spectrogram of corroded steel rod models, extra wave packets were found after the second wave packet. It represented the wave scattered by the surface rust and measured by the receiver; (5) Spectrograms at 1 MHz were used to compute TOF of ultrasonic waves. By considering only 1 MHz component, the dispersion effect during the propagation was eliminated; (6) Ultrasonic wave velocity at different path was estimated by Eq. (5); (7) Three equations were developed for the detection, location and quantification of surface rust. (i.e., Eq. (1), Eq. (7) and Eq. (4)). At last, a surface rust detection algorithm was developed based on above findings, as shown in Fig. 13.

4. CONCLUSION

This paper reports a study of point-source generated ultrasonic waves application on surface rust detection in a steel rod. Time domain radial displacement of ultrasonic waves propagating between transmitter and receiver

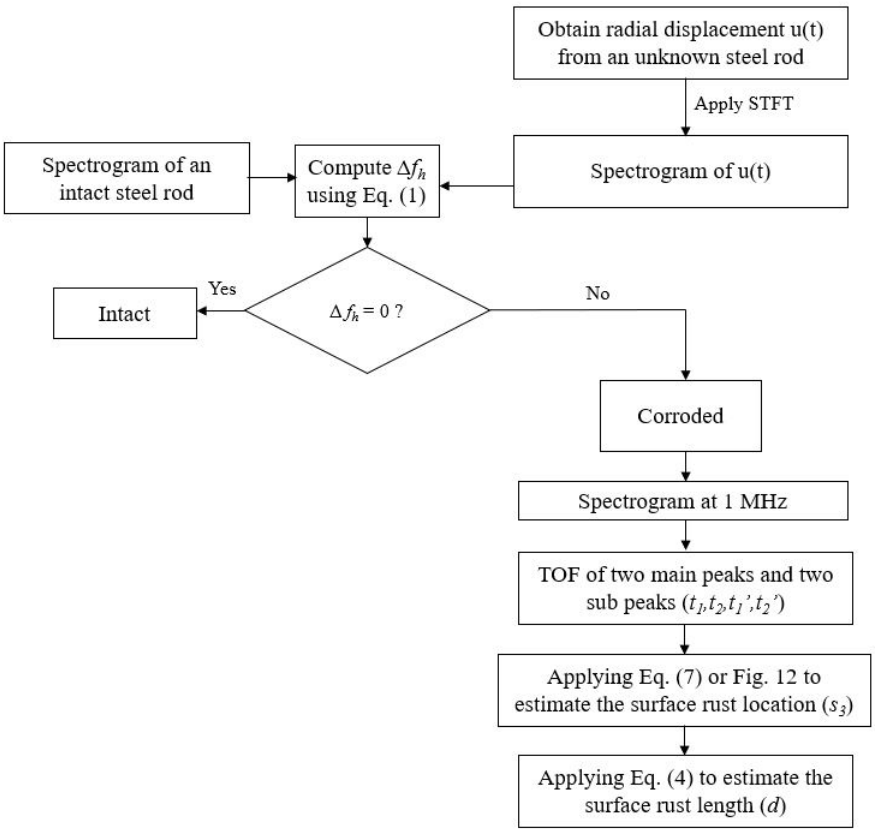

Figure 13. Surface rust detection algorithm

along the longitudinal direction and the helical direction is investigated. STFT is used for analyzing collected data. Presence of surface rust is detected by the reduction of high-frequency components in spectrograms. Surface rust location is estimated by using the difference between the arrival time of helical propagating ultrasonic waves and arrival time of scattered ultrasonic waves from surface rust. For surface rust length, the time delay of longitudinally propagated waves is used for estimation. It is believed that the proposed algorithm can be applied to surface rust detection algorithm for cylinder structures using point source ultrasonic waves.

5. ACKNOWLEDGMENT

The authors would like to thank the National Science Foundation (NSF), Division of Civil, Mechanical and Manufacturing Innovation (CMMI) for partially supporting this research through Grant CMMI-1401369.

REFERENCES

[1] Cook, D. and Berthelot, Y., "Detection of small surface-breaking fatigue cracks in steel using scattering of rayleigh waves," NDT E International 34, 483–492 (2001).

[2] Resch, M. T. and Nelson, D. V., "An ultrasonic method for measurement of size and opening behavior of small fatigue cracks," Small-crack test methods. ASTM International, , 169–196 (1992).

[3] Zou, X., Chao, A., Tian, Y., Wu, N., Zhang, H., Yu, T., and Wang, X., "An experimental study on the concrete hydration process using fabryperot fiber optic temperature sensors," Measurement 45 (2012).

[4] Zou, X., Chao, A., Tian, Y., Wu, N., , Yu, T., and Wang, X., "A novel fabry-perot fiber optic temperature sensor for early age hydration heat study in portland cement concrete," Smart Structures and System 12 (2013).

[5] Wu, N., Zou, X., Zhou, J., and Wang, X., "Fiber optic ultrasound transmitters and their applications," Measurement 79, 164–171 (2016).
[6] Tang, Q. and Yu, T., "Finite element simulation for damage detection of surface rust in steel rebars using elastic waves," Proceedings of SPIE Vol. 9804 (2016).
[7] Dassault Systémes, 10 rue Marcel Dassault, CS 40501, 78946 Vélizy-Villacoublay Cedex-France, Abaqus/CAE User's Manual Version 6.12.
[8] Liu, G. R. and Quek, S. S., "A non-reflecting boundary for analyzing wave propagation using the finite element method," Fn. Elem. in Anal. Des. 39, 403–417 (2003).
[9] Bergmann, L., "Ultrasonics and their scientific and technical applications," Wiley, New York (1948).